SEISMIC SOURCE AND PATH CALIBRATION IN THE KOREAN PENINSULA, YELLOW SEA, AND NORTHEAST CHINA

R. B. Herrmann[1], Y. S. Jeon[1], H.J. Yoo[2], K. H. Cho[2], W. R. Walter[3], and M. Pasyanos[3]

Saint Louis University[1], Seoul National University[2], and Lawrence Livermore National Laboratory[3]

Sponsored by National Nuclear Security Administration
Office of Nonproliferation Research and Development
Office of Defense Nuclear Nonproliferation

Contract Nos. DE-FC52-04NA25539[1,2] and W-7405-ENG-48[3]

ABSTRACT

The technique joint inversion of surface-wave dispersion and teleseismic P-wave receiver functions is used as a tool to derive a three-dimensional image of crustal velocities in the southern part of the Korean Peninsula. The station-specific surface-wave dispersion consists of two components—a long-period (10–150 s) Rayleigh-wave phase velocity dispersion for the peninsula and short period (0.5–20 s) tomographic Rayleigh- and Love-wave group velocity dispersion based on an analysis of >2100 empirical Green's functions derived from the cross-correlation of ground noise. When combined with teleseismic P-wave receiver functions from broadband, short-period, and acceleration sensors at 58 sites, a three-dimensional picture of the south Korean crust results. Spatial variations are seen in the depth to the Moho (28–32 km) and the degree of an upper crustal shear-wave velocity gradient from 3.0 to 3.5 km/s. Shear-wave velocities in the upper kilometer are typically greater than 3.0 km/s except in the southeast in the volcanoclastic Gyeongsang basin where the velocities are 5%–10% lower. An average velocity structure is used for moment tensor inversion.

OBJECTIVES

The primary focus is the determination of moment magnitudes for earthquakes in the Korean Peninsula, Yellow Sea and Northeast China region for use in calibration of coda based seismic moment determination. The source parameters are to be determined from the inversion of broadband waveforms of earthquakes in the region. To address the lack of large earthquakes, inversion of small earthquakes requires calibration of the shear-wave velocities in the upper crust in order to use the predominant signal in the higher frequency band of 0.05–0.2 Hz.

RESEARCH ACCOMPLISHED

Significant progress has been made in the characterization of the three-dimensional velocity structure of the southern half of the Korean Peninsula. Cho et al. (2006) mapped the variation of 1–20 s surface-wave group velocities in the study area. Yoo et al., (2006) used these and other surface-wave dispersion results together with teleseismic P-wave receiver functions at 80 sites to image the depth to the Moho and three-dimensional shear-wave velocity structure.

Study Area

The Korean Peninsula, Figure 1, situated at the eastern margin of the Eurasian continent, is a tectonic assemblage of two Phanerozoic mobile belts; the Imjingang belt and the Ogcheon fold belt, three Precambrian basement terrains; Nangrim, Gyeonggi, and Yeongnam Massifs from north to south, and one volcanoclastic basin, i.e., Gyeongsang basin (Chough et al., 2000). The Nangrim and the Gyeonggi massifs are separated by the Imjingang belt, which is a narrow suture zone recording high grade metamorphic events during the Late Permian to Early Triassic periods. The Gyeonggi and Yeongnam massifs are separated by the north-east trending Ogcheon belt, which is a fold and thrust belt involving Precambrian to Jurassic rocks. The Ogcheon belt and the Yeongnam massif contact at the Honam shear zone, north-east trending dextral strike-slip shear zone (ca. 400 km long and 80 km wide and both are overlain unconformably by Cretaceous sedimentary rocks). The volcanoclastic Gyeongsang basin covers the southeastern part of the Yeongnam massif. The tectonic affinity of the Korean Peninsula has been an enigma for a long time. The entire peninsula was traditionally regarded as an extension of the North China Block (also called the Sino-Korea Craton/Block). However, recent geological and petrophysical studies revealed that the Imjingang Belt and the Okchon Fold Belt (and Honam Shear Zone) could be the collision zone between the North China Block (Sino-Korea Craton) and the South China Block (Yangze Craton).

Digital Seismic Data

Digital seismology in Korea began with the installation of the Incorporated Research Institutions for Seismology (IRIS) station that is now at Inchon. Subsequently the Korean Institute of Geoscience and Mineral Resources (KIGAM) installed some broadband stations. In 2000, the Korean Meteorological Administration (KMA) digital seismic network became operational. The KMA network has a backbone of broadband stations, some additional short-period stations, and a dense network of accelerometers transmitting continuous data to the analysis center in Seoul. In addition, additional broadband sensors and accelerometers are operated by the Korean Electric Power Research Institute (KEPRI). For the surface-wave studies we used data from the broadband stations of KMA and KIGAM, approximately 15 at the time, for phase velocity determination, and waveforms from KMA broadband and acceleration channels for the group velocity analysis (Cho. et al., 2006). Receiver functions were determined from the KMA, KIGAM and KEPRI broadband channels and selected KMA short-period and acceleration channels. Figure 2 presents the location of the sites providing the group velocities and the receiver functions that we used in the study. The dense distribution of the stations permits us to examine the 3-D crustal structure in detail.

Surface-Wave Dispersion

The surface-wave data consists of two components. A peninsula average Rayleigh-wave phase velocity in the 10–50 s range, and tomographic estimates of the Rayleigh and Love wave group velocities in the 0.5–20 s period range determined using a 12.5 x 12.5 km grid for the southern part of the peninsula.

To obtain the phase velocities at longer periods, we applied the p-omega technique of McMechan and Yedlin (1981) to teleseismic Rayleigh waves observed on the Peninsula. The fundamental mode surface-wave was extracted using a combination of multiple filter analysis and phase matched filtering, a great circle path was assumed to project the

station observations onto a pseudo-linear array for analysis, and the phase velocities were determined. The Korean average Rayleigh wave phase velocity dispersion was determined in the 10–150 period range from about ten distant earthquakes. In spite of scatter, at the longer periods, the dispersion agreed with the Harvard tomography.

Cho K. H. et al. (2006) derived tomographic maps of Rayleigh- and Love-wave group velocity dispersion from inter-station empirical Green's functions obtained from the cross-correlation of ground noise (Shapiro et al., 2005). Group velocities were obtained from the empirical Green's functions for over 2100 inter-station paths in the 0.5–20 s period band. Because of the path density, they used a 12.5 x 12.5 km grid to create a tomographic dispersion image for each measured period. Figure 3 shows the Rayleigh-wave tomography results for selected periods. For our application, we associate the dispersion at a station with the nearest tomographic grid value. This is justified by the wavelengths considered and the smoothing used for the tomography. Figure 4 shows the dispersion data used at one KMA station, CHJ, for example.

Receiver Functions

Receiver functions are filters which predict a filtered version of a horizontal component from the vertical component trace (Ammon, 1997). This study uses P-wave radial receiver functions. To obtain these, teleseismic waveforms with a good P-wave signal are selected. The receiver function is estimated using the iterative time-domain deconvolution technique of Ligorria and Ammon (1999), which is an implementation of the Kikuchi and Kanamori (1982) technique. The time-domain Gaussian pulses used correspond to low-pass filters with frequencies of 0.3 and 1.0 Hz. Because of high-frequency noise, we did not attempt to use Gaussian filters with higher corner frequencies. In addition we did not try to use longer time-domain pulses, e.g., lower frequency data, because of long-period noise and because of the limited resolution of such data. In the terminology of Ligorria and Ammon (1999), we used the filter parameters alpha = 1.0 and 2.5.

A multi-step process was used to determine if a given receiver function should be used in the inversion for structure. The first criterion required that the derived receiver function predict 80% of the filtered radial signal power. This criterion is a quality check on the deconvolution stage. Given the large data sets and our unwillingness to subjectively exclude data, unrealistic receiver functions with the first pulse negative, passed this criterion since the deconvolution is a purely mathematical procedure that knows nothing of elastic wave propagation.

The second criterion involved using all acceptable receiver functions for the joint inversion of surface-wave dispersion and receiver functions at a station. The reduction of variance between each observed and predicted receiver function is obtained from this process. Predictions are made for the final crustal model and are thus constrained by elastic wave propagation theory. Of the receiver functions used, we used only those that fit 80% of the observed signal power. This stage rejected many signals for the final inversion. Of the 95 stations initially considered, only 80 stations had 2 or more good receiver functions. The locations of these stations are shown in Figure. 2a. Table 1 gives the station names, coordinates, and the final number of receiver functions used for the site.

We were able to have so many stations available for analysis because we obtained receiver functions from broadband (STS-2), short-period (SS-1) and acceleration (Episensor) channels of the 20 Hz archived data stream. Since STS-2 and SS-1 sites also had Episensor channels, we were able to verify that the acceleration channels could give good receiver functions. The possibility of using the acceleration channels was suggested by the success in obtaining empirical inter-station Green's functions from them, which is because these channels in Korea are more sensitive than is typical. The use of these data is made easier since there seems to be little azimuthal dependence on the receiver function and since the P-wave transverse receiver function is usually small.

Joint Inversion Structure

Joint inversion of receiver functions and surface-wave dispersion was first proposed by Özalaybey et al. (1997). It has been used by Juliá et al. (2000), Herrmann et al., (2001), Chang et al., (2004), and Chang and Baag (2005). The iterative least-squares joint inversion used here is described by Herrmann and Ammon (2002). Surface-wave dispersion partial derivatives are computed analytically while receiver function partial derivatives are computed numerically. The inversion fixes the Vp/Vs ratio in each layer and recomputes layer density from the P-wave velocity after each iteration. A differential smoothing constraint is applied with the objective of finding the simplest model that fits the data set. The smoothing constraint is implemented by solving for the change in the velocity

contrast at layer boundaries rather than solving for the changes in the individual layer velocities. The starting model used at all sites consists of 85 layers to a depth of 580 km. From a depth of 50 km to the bottom, the model is AK135-F Continental Model (http://wwwrses.anu.edu.au/seismology/ak135/ak135f.html). The upper 50 km of the model consists of layers (four 1 km and twenty-three 2 km) having the same velocities as AK135-F at 50 km. The velocity jumps at the layers boundaries are not permitted to change from 380 km to the bottom of the model. They are permitted to change slightly from 80–380 km, and they are permitted to change in the upper 80 km. The high initial velocities of the crust provide a uniform unbiased starting model for the inversion. No a priori assumptions about the location of the Moho are made. In addition no persistent artifacts of crustal layer boundaries appear in the solution. Starting with a continental upper mantle, and permitting a significant departure from the starting model only in the upper 80 km, ensure that the lower part of the model does not depart from the global seismology experience. The choice of crustal layer thicknesses of 2.0 km is appropriate because of the lack of resolution with fundamental mode surface-wave dispersion, and the receiver function resolution for the filters used.

As mentioned above, we performed the joint inversion twice, first with all receiver functions associated with a successful deconvolution, and second with just those for which the model provided at least an 80% variance reduction in fit. Since it is the receiver functions, which provide the constraints on velocity model discontinuities, we will focus only on those 80 sites which had 2 or more receiver functions. At common stations, we have compared our inverted models with those from the recent work of Chang et al. (2004) and Chang and Baag (2005). The models are similar.

Rather than presenting all 80 crustal models, and to test the usefulness of our approach to image the three-dimensional crust, we present the results as a contour map of Moho depth and vertical sections. Presenting the Moho depth estimates as a contoured surface is a compromise because the Moho probably does not change in depth as a smoothly varying surface everywhere, but it presents the most effective means to view the data. To make the Moho contour map, we assign the Moho where the shear wave velocity increases to or is >4.2 km/s in each model and then applied “minimum curvature technique” (Smith and Wessel, 1990) for interpolation. The Moho depth varies from about 26 km to 38 km and 32.7 km in average (Figure 5). It is deeper in the southern and central parts of the peninsula. It is to be noted that the variation of Moho topography of the east coast differs from that of the west and south coasts. Figure 6 shows representative two-dimensional crustal shear-wave velocity slices along diagonal paths across the study area.

MOMENT TENSOR INVERSIONS

Using the moment tensor inversion techniques and velocity model developed for SRR 2005, we have continued to use regional broadband waveforms for the determination of earthquake source parameters for earthquakes in the study region. Our tabulation now consists of solutions for 27 earthquakes and is available at the web page

http://www.eas.slu.edu/Earthquake_Center/MECH.KR/

As additional earthquakes occur, we will include them in this tabulation.

CONCLUSION(S) AND RECOMMENDATIONS

The striking difference between the Moho depth in the southern and eastern parts of the peninsula reflect the tectonic origins the crust. A working hypothesis is that the velocity models derived in the northwestern part of South Korea may be applicable to the entire northern part of the peninsula. The previously reported model for waveform inversion for source properties still applies.

ACKNOWLEDGEMENTS

Maps were created using Generic Mapping Tools, or GMT (Wessel and Smith, 1995).

REFERENCES

Ammon (1997). An overview of receiver-function analysis, http://eqseis.geosc.psu.edu/~cammon/HTML/RftnDocs/rftn01.html.

Ammon, C. J., G. E. Randall, and G. Zandt (1990). On the nonuniqueness of receiver function analysis, *J. Geophys. Res.* 95: 15,303–15,318.

Chang, S. and C. Baag (2005). Crustal Structure in southern Korea from joint analysis of teleseismic receiver functions and surface-wave dispersion, *Bull. Seism. Soc. Am.* 95: 1,516–1534.

Chang, S., C. Baag, and C. A. Langston (2004). Joint analysis of teleseismic receiver functions and surface wave dispersion using the genetic algorithm, *Bull. Seism. Soc. Am.* 94: 691–704.

Cho, H.-M., C.-E. Baag, J. M. Lee, W. M. Moon, H. Jung, K. Y. Kim, and I. Asudeh (2006). Crustal velocity structure across the southern Korean Peninsula from seismic refraction survey, *GRL* 33: L06307, doi:10.1029/2005/GL025145.

Cho, K. H., R. B. Herrmann, C. J. Ammon, and K. Lee (2006). Imaging the upper crust of the Korean Peninsula by surface-wave tomography, *Bull. Seism. Soc. Am.* (in review).

Chough, S. K., S.-T. Kwon, J.-H. Ree, and D. K. Choi (2000). Tectonic and sedimentary evolution of the Korean peninsula: a review and new view, *Earth-Sci. Rev.* 52: 175–235.

Herrmann, R. B., C. J. Ammon, and J. Juliá (2001). Application of joint receiver-function surface-wave dispersion for local structure in Eurasia, in *Proceedings of the 23rd Seismic Research Review: Worldwide Monitoring of Nuclear Explosions*, LA-UR-01-4454, Vol. 1, pp. 46–54.

Kikuchi, M. and H. Kanamori (1982). Inversion of complex body waves, *Bull. Seism. Soc. Am.* 72: 491–506.

Juliá, J., C. J. Ammon, R. B. Herrmann, and A. M. Correig (2000). Joint inversion of receiver function and surface wave dispersion observations, *Geophys. J. Int.* 143: 99–112.

Ligorria, J. P. and C. J. Ammon (1999). Iterative deconvolution of teleseismic seismograms and receiver function estimation, *Bull. Seism. Soc. Am.* 89: 1,395–1,400.

McMechan, G. A. and M. J. Yedlin (1981). Analysis of dispersive waves by wave field transformation, *Geophys.* 46: 869–874.

Min, K. and M. Cho (1998). Metamorphic evolution of the northwestern Ogcheon metamorphic belt, South Korea, *Lithos* 43: 31–51.

Özalaybey, S., M. K. Savage, A. F. Sheehan, J. N. Louie, and J. N. Brune (1997). Shear-wave velocity structure in the northern Basin and Range province from the combined analysis of receiver functions and surface waves, *Bull. Seism. Soc. Am.* 87: 183–199.

Shapiro, N. M. M. Campillo, L. Stehly, and M. H. Ritzwoller (2005). High resolution surface wave tomography from ambient seismic noise, *Science* 307: 1,615–1,618.

Smith, W. H. F. and P. Wessel (1990). Gridding with continuous curvature splines in tension, *Geophys.* 55: |293–305.

Wessel, P. and Smith, W. (1995). New version of the generic mapping tools released. *EOS Trans. AGU* 76: 329.

Yoo, H. J., R. B. Herrmann, K. H. Cho, and K. Lee (2006). Imaging the three-dimensional crust of the Korean Peninsula by joint inversion of surface-wave dispersion and teleseismic receiver functions, *Bull. Seism. Soc. Am.* (in review).

Table 1. Station locations and number of receiver functions used

Sta	Lat	Lon	N	Sta	Lat	Lon	N	Sta	Lat	Lon	N
KWJ	35.16	126.99	156	HDB	35.73	129.40	21	IMS	35.61	127.29	7
HUK	34.68	125.45	139	GKP1	35.89	128.61	21	HAC	35.56	128.17	7
DGY	37.69	128.67	136	SWO	37.27	126.97	15	DDC	37.89	127.06	7
AND	36.57	128.71	128	BRD	37.97	124.63	15	MAS	35.17	128.57	6
CHC	37.78	127.81	113	SKC	38.29	128.52	14	HOC	37.68	127.88	6
CHO	35.82	127.15	107	BUS	35.25	129.11	13	BUY	36.27	126.92	5
DAG	35.77	128.90	104	INJ	38.05	128.17	11	CWO	38.08	127.52	5
YGN	35.40	126.42	83	YOW	37.17	128.46	10	MOP	34.81	126.38	5
CHI	35.20	128.12	75	ULC	36.99	129.41	10	TOH	37.50	129.12	5
UCN	37.08	129.38	70	SOS	36.78	126.49	10	YAP	37.48	127.49	5
PUS	35.10	129.03	63	CPN	36.22	127.99	10	CHY	36.94	128.92	4
SES	36.79	126.45	60	CEA	36.82	127.26	10	KOH	34.61	127.27	4
SEO	37.49	126.92	56	WON	37.33	127.94	9	KUJ	34.88	128.60	4
ULJ	36.70	129.41	47	HAN	34.57	126.57	9	KUM	36.12	128.32	4
TJN	36.38	127.36	42	EUS	36.35	128.69	9	MIY	35.49	128.74	4
CHU	37.89	127.73	40	YJD	37.47	126.43	8	NAW	35.40	127.33	4
WSN	35.72	129.47	36	YOS	34.74	127.74	8	SUC	35.07	127.24	4
KAN	37.74	128.89	36	YOD	36.53	129.41	8	YOC	35.97	128.95	4
TEJ	36.37	127.37	35	POR	36.32	126.56	8	CEJ	36.64	127.44	3
SNU	37.45	126.96	34	JEC	37.15	128.19	8	PHA	36.19	129.37	3
KRN	35.33	129.30	33	CHA	36.77	127.12	8	BGD	34.16	126.56	2
TAG	35.88	128.62	32	WAN	34.39	126.70	7	BOE	36.49	127.74	2
KUC	35.67	127.91	32	ULS	35.55	129.32	7	KMS	36.10	127.48	2
KUS	36.02	126.83	30	NAH	34.82	127.93	7	PUA	35.72	126.72	2
CHJ	36.87	127.98	25	MUS	37.89	126.76	7	SAC	35.41	127.88	2
JEU	35.49	126.93	23	MUG	36.62	128.15	7	TOY	34.85	128.44	2
ICN	37.29	127.42	23	JAH	34.69	126.92	7				

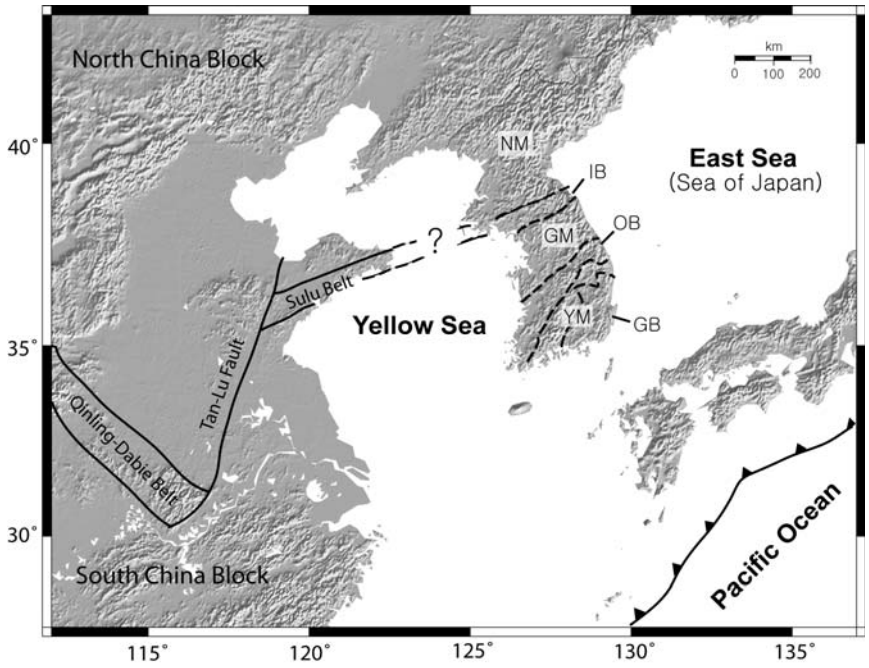

Figure 1. Tectonic map of the Korean Peninsula and adjacent area (modified from Min and Cho, 1998; Chough et al., 2000). Major tectonic provinces are separated by dashed lines. NM, Nangrim massif; GM, Gyeonggi massif; YM, Yeongnam massif; IB, Imjingang belt; OB, Ogcheon fold belt; GB Gyeongsang basin. The topography is from ETOPO02.

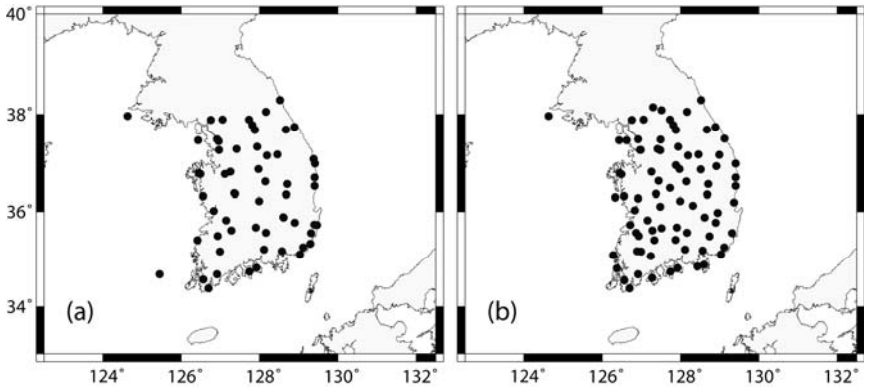

Figure 2. Location of stations used in this study. (a) Stations used for receiver function determination. (b) Stations used for group velocity determination from inter-station Green's functions from the cross-correlation of seismic noise.

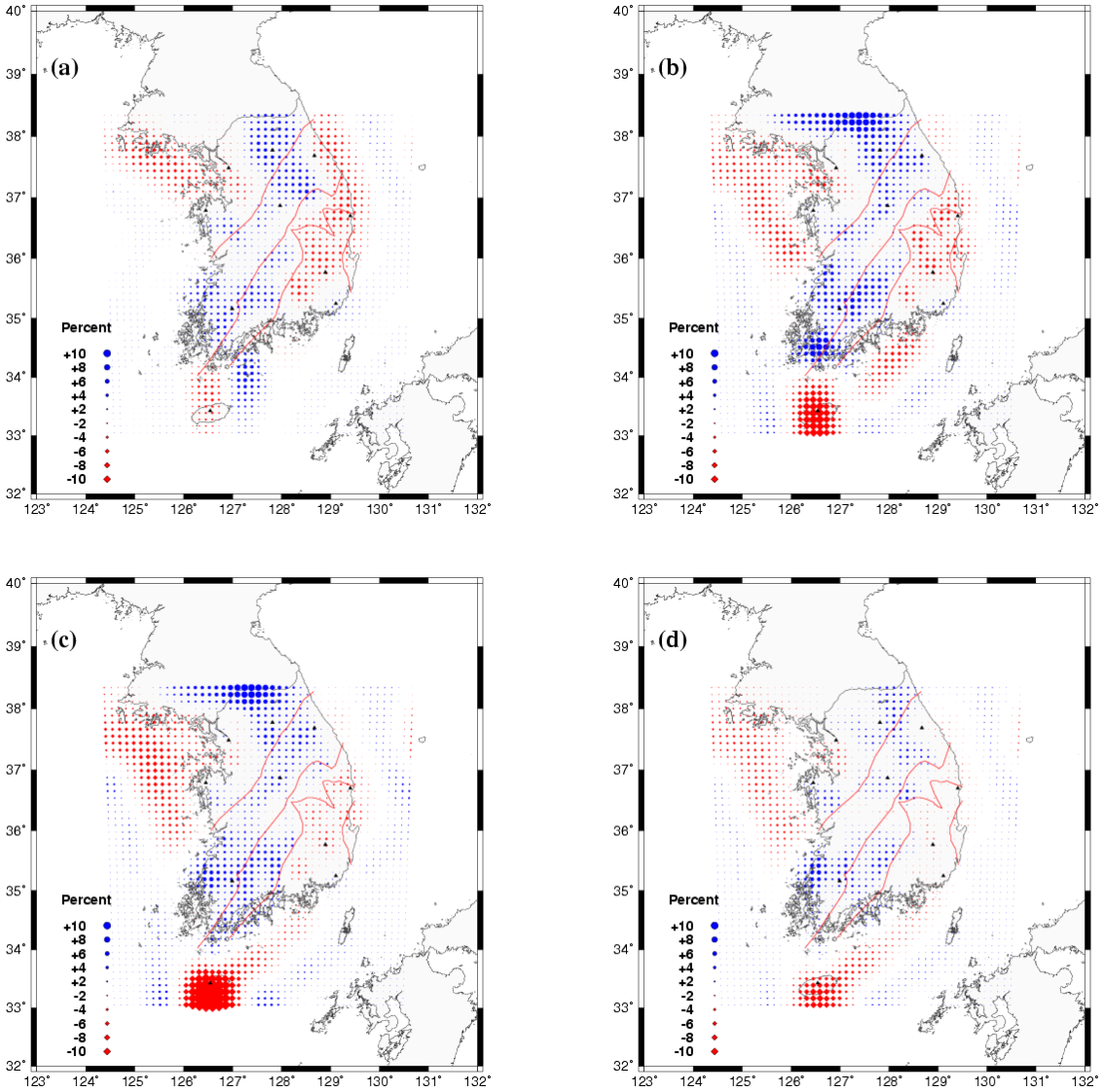

Figure 3. Rayleigh-wave group velocity tomography results for periods of 1.0 (a), 2.0 (b), 3.0 (c) and 6.0 (d) seconds. The boundary lines on the Peninsula separate the major tectonic units Gyeonggi massif, Okcheon fold belt, Yeongnam massif and Gyeongsang basin (Chough et al, 2000; Cho, H.M. et al., 2006).

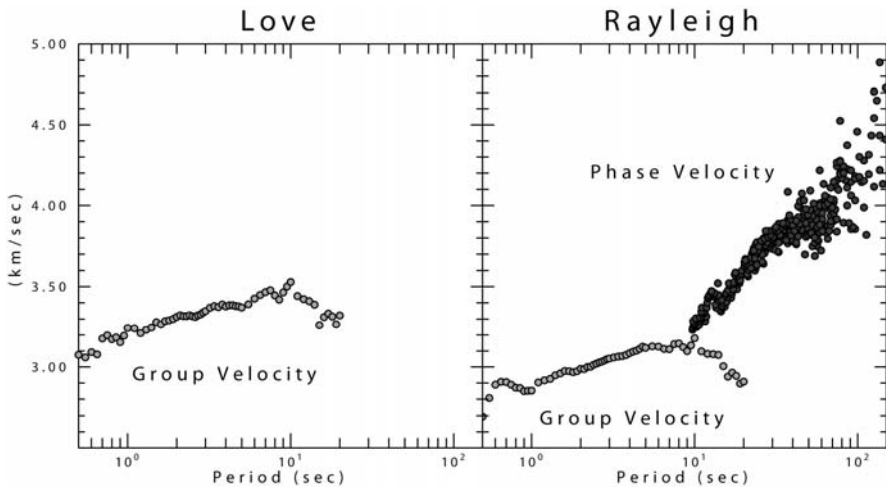

Figure. 4. Dispersion data used for the station CHJ (36.87N, 127.97E). The group velocities are indicated by the lighter shade of gray, and the phase velocities by the darker.

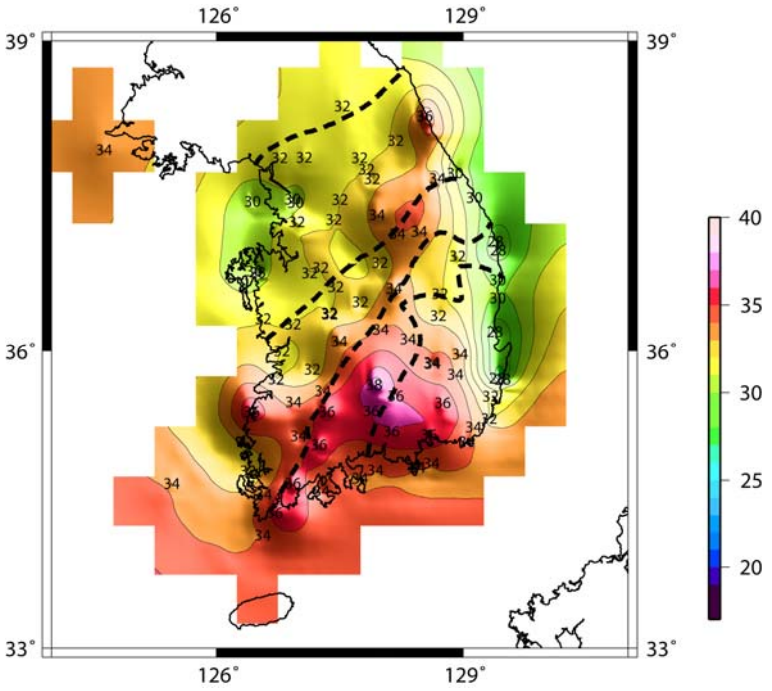

Figure 5. Distribution of the Moho depths in southern Korean Peninsula. Interplolation is performed using "minimum curvature technique" (Smith and Wessel, 1990). Locations and Moho depths used in the interpolation are shown in the map. Major tectonic boundaries are shown as dashed lines.

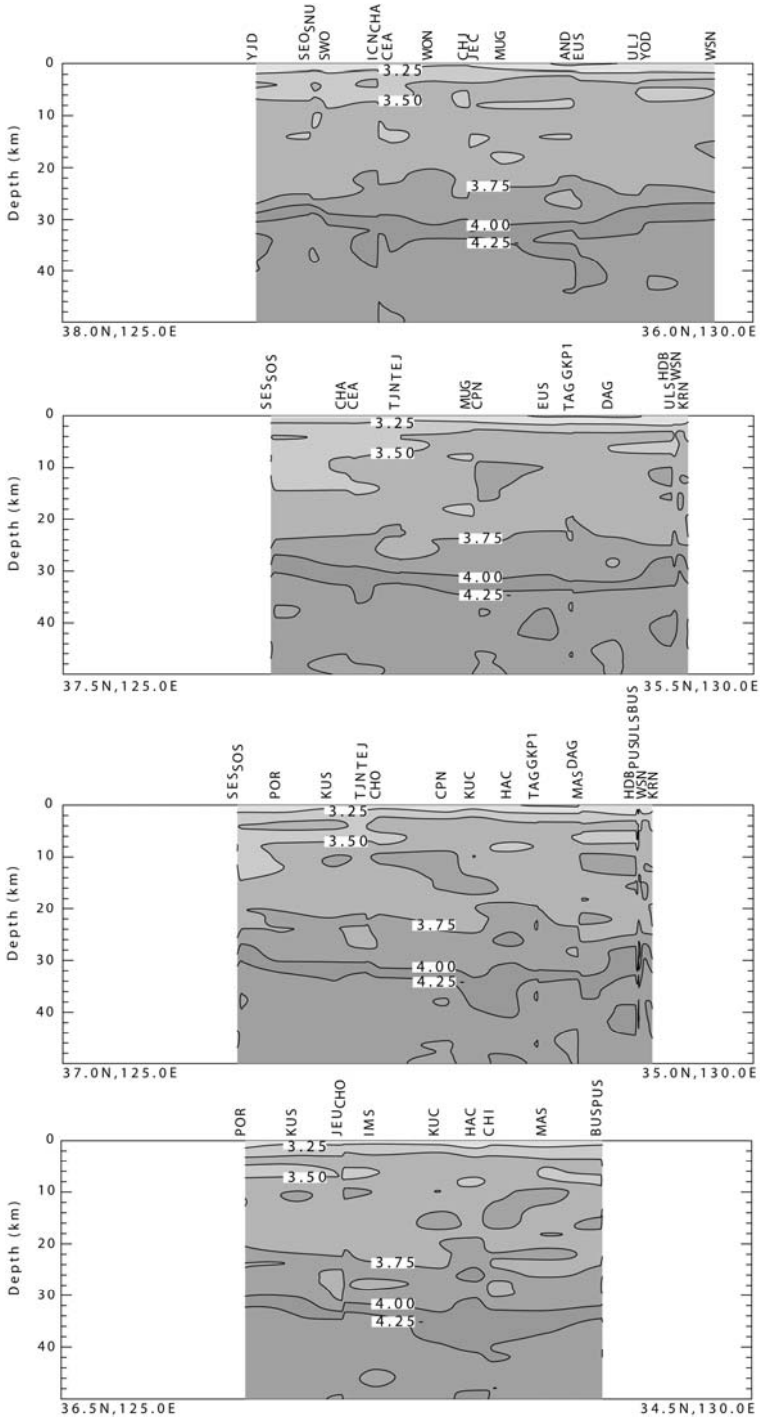

Figure 6. Northwest-southeast diagonal shear-wave velocity profiles across the study area arranged from north to south. The coordinates of the profile are given at the bottom of each plot. Contours are given at every 0.25 km/s and the 3.00 to 4.25 km/s contours are indicated.